https://doi.org/10.2352/ISSN.2470-1173.2017.17.COIMG-422

Fast and Robust Discrete Computational Imaging

Ahmet Tuysuzoglu; Siemens Medical Solutions USA, Inc., Princeton, NJ
Yuehaw Khoo; Stanford University; Palo Alto, CA
W. Clem Karl; Boston University; Boston, MA

Abstract

Computational imaging problems are of increasing importance in domains ranging from security to biology and medicine. In these problems computational techniques based on an imaging model are coupled with data inversion to create useful images. When the underlying desired property field itself is discrete, the corresponding discrete-valued inverse problems are extremely challenging and computationally expensive to solve because of their non-convex, enumerative nature. In this work we demonstrate a fast and robust solution approach based on a new variable splitting coupled with the alternating direction method of multipliers (ADMM) technique. This approach exploits sub-problems that can be solved using existing and fast techniques, such as graph-cut methods, and results in overall solutions of excellent quality. The method can exploit both Gaussian and Poisson noise models. We exercise the method on both binary and multi-label phantoms for challenging limited data tomographic reconstruction problems.

INTRODUCTION

In computational imaging problems data is combined with an imaging model to yield an image obtained as the computational solution of an inverse problem. An interesting and challenging sub-class of these problems arises when the underlying property field is constrained to be discrete valued. This situation can arise when the domain is constrained to be discrete (e.g. imaging a few materials with known values) or because of interest in higher level information (e.g. labels). For example, limited angle tomography problems involving only a few attenuation values commonly exist in electron tomography of materials where the aim is to visualize the 3D structure of a sample [1]. In these cases, the corresponding discrete-valued inverse problems are extremely challenging and computationally expensive to solve due to their non-convex and enumerative nature.

One simple, conventional approach to such problems is to solve the computational imaging inverse problem ignoring the discrete nature of the scene, and then, subsequently, impose discreteness through rounding or projection. Conventional continuous solution methods (e.g. gradient techniques) can then be applied. In cases with limited or poor quality data the initial continuous inversion step can produce reconstructions containing significant artifacts and make any subsequent segmentation and quantitation of the result very challenging. Direct solution of the discrete problem can produce significantly improved overall results in these challenging scenarios.

A number of different approaches have been proposed for the solution of the discrete tomographic image reconstruction problem. Linear programming relaxations of the binary tomography problem were used in [2, 3] where the latter work employed a smoothness prior. Batenburg *et al*. [4] proposed an iterative algorithm called discrete algebraic reconstruction technique (DART) that makes use of successive steps of algebraic reconstruction and segmentation. The key idea behind DART is to fix and remove the set of pixels that are deemed to be correctly segmented from the set of observation equations which improves the conditioning of the resulting linear system. A row action method then acts on just those pixels that were not correctly segmented in the previous iteration. Although DART has been shown to perform well under low-noise scenarios, the lack of a principled regularization component hampers its performance under more challenging sensing scenarios. In order to improve the performance of DART under noisy scenarios, an extension named SDART was presented in [5]. SDART uses a penalty function to enforce the closeness of the segmented image to the continuous-valued image at each iteration of the algorithm. The penalty function is determined using confidence measures derived from the reconstructed images. It has been demonstrated through experimentation that SDART can perform better in noisy scenarios than DART.

The above techniques relax the discrete field constraints to obtain tractable solution methods. There also exists methods that directly minimize a regularized reconstruction functional over a combinatorial discrete set of values by employing graph-cuts techniques. Graph-cut methods have shown themselves to be efficient tools for obtaining solutions to segmentation and label-based optimization problems [6]. But these approaches have had limited use in inverse problem contexts because of the coupled variable structure induced by the sensing operators of corresponding computational imaging problems, which prohibit their direct mapping to a graph-cut problem. Examples of work in this direction includes the work of Raj *et al*. [7], where a surrogate energy function is dynamically constructed for problems with non-negative system matrices and the work of Kolmogorov and Rother [8], where variable relabeling is used to minimize non-graph representable functionals. Unfortunately, many pixels can be left unlabeled if the sensing operator induces pixel coupling, as occurs for tomography.

Recent work has made progress, however. In [9] a dual formulation for the binary tomographic reconstruction is proposed, where the observation model is used as a set of linear constraints to an integer program, thus avoiding quadratic terms. In addition, the discrete regularized reconstruction problem was analyzed in [10] with respect to submdoularity and an iterative surrogate minimization framework that can be mapped as a graph-cut problem was proposed. Extensive experimentation showed that this algorithm performed better than DART and other competing tech-

This feature is based on research, and is not commercially available. Due to regulatory reasons its future availability cannot be guaranteed.

niques under noisy data situations.

This paper further examines the discrete tomographic framework presented in [11]. The framework in [11] directly formulates discrete computational imaging problems in the discrete domain and then solves the resulting challenging inverse problem through a variable splitting coupled with the alternating direction method of multipliers (ADMM) framework. This approach is versatile, inherently discrete, and allows the use of efficient solvers at each step of the algorithm. In this work we extend the analysis of [11] by presenting reconstruction results for sparse tomographic data scenarios.

Reconstruction Framework

Observation Model

In modeling discrete-valued computational imaging problems, an unknown image, represented by the n-dimensional vector $\mathbf{x}$, is related to a set of observed data, represented by the m-dimensional vector $\mathbf{y}$, through a linear operator, represented by the $m \times n$ matrix $\mathbf{C}$:

$$\mathbf{y} = \mathscr{N}(\mathbf{C}\mathbf{x}), \tag{1}$$

where $\mathscr{N}$ represents the effects of a noise operator. Equation (1) is our general observation model. For the purposes of this work we focus on two different observation noise models discussed in further detail below: additive Gaussian noise and signal dependent Poisson noise.

Discrete Image Creation Framework

We obtain an estimate of the underlying image as the solution of an inverse problem. In particular, a reconstructed image is obtained as the minimizer of an energy function that captures the problem elements we deem significant:

$$\underset{\mathbf{x}}{\operatorname{argmin}} J(\mathbf{x}) \text{ such that } \mathbf{x} \in \mathscr{L}^n, \tag{2}$$

where $\mathbf{x} \in \mathscr{L}^n$ captures the constraint that the values in $\mathbf{x}$ are constrained to be in the discrete set of pixel values $\mathscr{L} = \{l_1, \ldots, l_L\}$. We assume that the $|\mathscr{L}|$-levels l_i of the image are known. The energy $J(\mathbf{x})$ is composed of two terms:

$$J(\mathbf{x}) = J_{\text{data}}(\mathbf{x}) + \lambda J_{\text{prior}}(\mathbf{x}), \tag{3}$$

where the regularization parameter λ balances the trade-off between the two terms. The first term in the objective function, $J_{data}(\mathbf{x})$, represents the fidelity to the observed data. We set this term to be proportional to the negative log-likelihood of the data based on the noise model under consideration, as shown in Table 1. The second term $J_{\text{prior}}(\mathbf{x})$ represents a regularizer that promotes stable solutions and incorporates prior information on the behavior of the reconstructed discrete-valued field. A variety of choices are possible for this term. In this work we use a continuity or smoothness prior capturing the fact that for many problems nearby pixel values are similar:

Gaussian Noise $J_{\text{data}}(\mathbf{x}) =$	Poisson Noise $J_{\text{data}}(\mathbf{x}) =$
$\|\mathbf{y} - \mathbf{C}\mathbf{x}\|_2^2$	$\sum_{i=1}^{m} I_0 e^{-[\mathbf{C}\mathbf{x}]_i} + \mathbf{y}_i [\mathbf{C}\mathbf{x}]_i$

Noise-based data penalties $J_{\text{data}}(\mathbf{x})$

$$J_{\text{prior}}(\mathbf{x}) = \sum_{\substack{(p,q)\in\mathscr{B} \\ p<q}} |\mathbf{x}_p - \mathbf{x}_q|, \tag{4}$$

where $\mathscr{B}$ defines a neighborhood structure among pixels. The prior can be equivalently formulated using a discrete difference operator $\mathbf{D}$ as follows:

$$J_{\text{prior}}(\mathbf{x}) = \|\mathbf{D}\mathbf{x}\|_1^1. \tag{5}$$

We assume an 8-connected neighborhood in this work.

Since the energy functional given in (2) depends on a variables that take on a discrete set of values, conventional gradient-based methods cannot be utilized, rendering minimization challenging and requiring a different approach than brute force application of existing tools.

Algorithm: Variable Splitting and ADMM

In this section we review the new reconstruction framework presented in [11], summarizing the development therein. The difficulty of minimizing Eq. 3 stems from the fact it has to be minimized over a set that is combinatorially large. Furthermore, the variables are coupled due to the operator $\mathbf{C}$, making straightforward use of existing discrete optimization tools impossible. To overcome these challenges in [11] the original optimization problem given in Eq. 3 is recast using a particular variable splitting to obtain the following equivalent formulation:

$$\begin{aligned} &J_{\text{SPL}}(\mathbf{x},\mathbf{z}) = J_{\text{data}}(\mathbf{x}) + \lambda \|\mathbf{D}\mathbf{z}\|_1^1 \qquad \text{(SPL)} \\ &\text{such that } \mathbf{x} = \mathbf{z},\ \mathbf{z} \in \mathscr{L}^n, \mathbf{x} \in \mathscr{R}^n. \end{aligned}$$

Note that this choice of variable splitting places a continuous variable in the coupled data penalty and a discrete variable in the smoothness-based regularizer. With this new splitting the Alternating Direction Method of Multipliers (ADMM) from the field of convex optimization is now applied to solve problem SPL efficiently.

The particular variable splitting in (SPL) brings problem (2) into the general ADMM form, except that (SPL) is a non-convex problem due to the discrete constraint on $\mathbf{z}$. While the guaranteed properties of ADMM are lost in such cases, the application of ADMM to non-convex problems has proved successful in solving other non-convex problems [12, 13, 14] in practice. In the present case, the individual updates in the ADMM-based algorithm can be solved for optimally and efficiently. The steps for the TOMO-SPL algorithm are given as follows [11]:

$$\mathbf{x}^{k+1} = \underset{\mathbf{x}\in\mathbf{R}^n}{\operatorname{argmin}} J_{\text{data}}(\mathbf{x}) + (\rho/2)\|\mathbf{x} - \mathbf{z}^k - \mathbf{u}^k/\rho\|_2^2, \tag{6}$$

$$\mathbf{z}^{k+1} = \underset{\mathbf{z}\in\mathscr{L}^n}{\operatorname{argmin}} \lambda\|\mathbf{D}\mathbf{z}\|_1^1 + (\rho/2)\|\mathbf{x}^{k+1} - \mathbf{z} - \mathbf{u}^k/\rho\|_2^2, \tag{7}$$

$$\mathbf{u}^{k+1} = \mathbf{u}^k - \tau\rho(\mathbf{x}^{k+1} - \mathbf{z}^{k+1}). \tag{8}$$

For the noise models of interest here, the solution of 6 can be obtained in closed-form or via conventionally efficient iterative methods. The problem in 7 represents a discrete optimization problem of conventional form, since the variable mixing due to the operator has been eliminated. In particular, powerful graph-cut methods can be applied. Lastly, the update in 8 is simple. In the next subsections we review the individual updates.

x-update: Additive Gaussian noise model

The additive, white Gaussian model is given as follows:

$$\mathbf{y} = \mathbf{C}\mathbf{x} + \mathbf{n}, \tag{9}$$

where $\mathbf{n}$ represents the noise vector of size m drawn from independent and identically distributed Gaussian random variables. For the additive, Gaussian noise case the data-fidelity term is simply:

$$J_{\text{data}}(\mathbf{x}) = \|\mathbf{y} - \mathbf{C}\mathbf{x}\|_2^2. \tag{10}$$

The update with respect to $\mathbf{x}$ amounts to solving the following set of normal equations:

$$\left(\mathbf{C}^T\mathbf{C} + \frac{\rho^2}{4}I\right)\mathbf{x} = \mathbf{C}^T\mathbf{y} + \frac{\rho^2}{4}\mathbf{z}^k + \frac{\rho}{4}\mathbf{u}^k. \tag{11}$$

Many efficient linear solvers exist. Here we use the conjugate gradient method initializing with $\mathbf{x}^t$.

x-update: Poisson noise model

Under a Poisson noise model each observation, $\mathbf{y}_i$, is sampled from the Poisson random variable Y_i,

$$Y_i \sim \text{Poiss}\left(I_0 e^{-[\mathbf{C}\mathbf{x}]_i}\right), \tag{12}$$

where I_0 is the blank scan factor. The data-fidelity term is obtained from the negative log-likelihood and is given by:

$$J_{\text{data}}(\mathbf{x}) = \sum_{i=1}^{m} I_0 e^{-[\mathbf{C}\mathbf{x}]_i} + \mathbf{y}_i[\mathbf{C}\mathbf{x}]_i. \tag{13}$$

The $\mathbf{x}$ update step can be interpreted as computing the Poisson maximum likelihood estimator coupled with a simple regularizer, for which many efficient solvers exist.

z-update: Submodular minimization

The $\mathbf{z}$ update step amounts to solving the so called discrete total-variation problem. The problem is submodular and can be solved globally both in the binary and multi-label cases. Furthermore there exists algorithms that solve this problem in the complexity of a single maximum-flow computation, regardless of the number of labels [15]. Here we use the FAST PD algorithm [16, 17].

Convergence, Parameter Selection and Stopping Criterion

The ADMM framework has two parameters that need to be defined. The first is the penalty parameter ρ, which affects the rate of convergence. In convex problems, the penalty parameter ρ is generally picked between $(0, (1+\sqrt{5})/2)$ for convergence [18]. Furthermore it is customary to adjust ρ during the iterations. In nonconvex problems the situation is more complex [12]. We have empirically observed that for the algorithm in [11], increasing ρ is important for convergence. We illustrate this in Fig. 1 (b), where convergence with respect to fixed ρ and increasing ρ are compared. The particular choice of ρ and the increase rate are detailed in the experimental section. We further note that ρ and its increase rate can be picked from a fairly large range without affecting the overall convergence. Therefore, we use the same set of parameters throughout a diverse set of experiments.

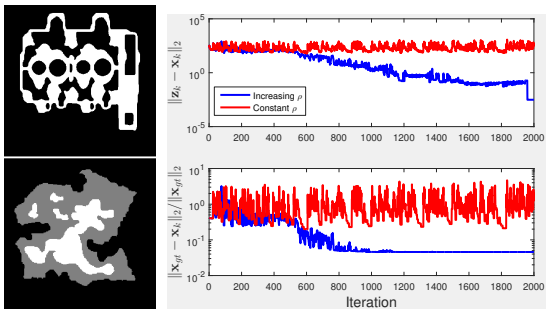

(a) (b)

Figure 1. *(a) Images used in the experiments. Top row: Binary phantom, bottom row: Multi-label phantom. (b) Convergence plots with (blue) and without (red) increasing ρ. Top row: Norm of primal feasibility, $\|\mathbf{x}_k - \mathbf{z}_k\|_2$. Bottom row: Normalized distance of $\mathbf{x}_k$ to ground truth, $\|\mathbf{x} - \mathbf{x}_k\|_2/\|\mathbf{x}\|_2$. The y-axis is shown in logarithmic scale.*

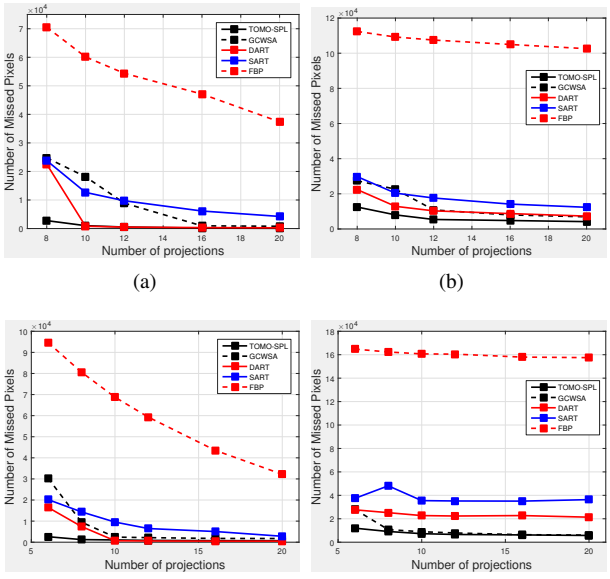

(a) (b)

(c) (d)

Figure 2. *Performance of TOMO-SPL (solid black), GCWSA (dashed black), DART (solid red), SART (solid blue), FBP (dashed red) with varying number of projections: Binary phantom (a) without noise, (b) with noise. Multi-label phantom (c) without noise (d) with noise.*

Experiments

Sparse and limited angle acquisition scenarios pose a challenge for existing continuous and discrete reconstruction algorithms. In our experiments we focus on these challenging data collection scenarios using simulated data. The simulated data has been generated using the ASTRA toolbox [19]. In our experiments the width of the sensor array was set to 1.5 times of the image size and the sensor size was set to be same as the pixel size. We compare the performance of the proposed method which we call TOMO-SPL, with the baseline techniques, filtered back projection (FBP), simultaneous algebraic reconstruction technique (SART) and the discrete algebraic reconstruction technique (DART) [20] and the graph-cuts with separable approximation (GCWSA) method [10]. We use the publicly available

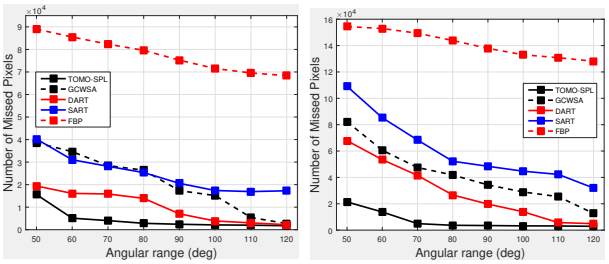

(a) (b)

Figure 3. *(a) Performance of TOMO-SPL (solid black), GCWSA (dashed black), DART (solid red), SART (solid blue), FBP (dashed red) with changing angular range under noise: (b) Binary phantom, (c) Multi-label phantom.*

implementations of the first three methods as provided in the ASTRA toolbox. We evaluate the performance of the proposed technique using binary and multi-label phantoms of size 512×512 that are adapted from [4] as shown in Fig 1 (a).

For all methods used, we optimized their parameters (if there is any) by manual tuning. The DART was run 200 iterations where we set the percentage of random points to 0.1 and 0.4 for noise-free and noisy sensing scenarios respectively and smoothing intensity to 0.2. In [4], it was shown that increasing the number of random points is helpful when there is observation noise. TOMO-SPL was run with an initial ρ of 10 and we increased ρ with a factor of 1.005 at every iteration. The iterations were stopped when the primal residual dropped below 10^{-2}. SART was run with nonnegativity constraints for 100 and 200 iterations for noisy and noiseless cases respectively and FBP results were thresholded to eliminate negative pixel values with zeros. FBP and SART reconstructions are segmented with Otsu's thresholding technique [21] before counting the number of missed pixels. All methods that required initialization was initialized with an all zeros image. Regularization parameter selection for GCWSA and TOMO-SPL was based on visual judgement. The label set for each experiment was assumed to be known for a priori.

Sparse Angle Experiments

We sample the the full angular range equidistantly to simulate sparse angle data collection experiments. We first start with a noise-free sensing scenario. The performance plots illustrating the number of misclassified pixels for each of the compared techniques are shown in Fig. 2 (a) and (c) for the binary and multi-label phantoms, respectively. Although DART and GCWSA show similar performance to TOMO-SPL when there are enough projections, TOMO-SPL outperforms them when data is scarce. We show example reconstructions with 8 projections for the binary phantom and 6 for the multi-label phantom in Fig. 4. For the binary phantom, TOMO-SPL was able to generate a faithful representation whereas the other techniques techniques failed to do so. This observation is in agreement with the results presented in the DART paper [4] where they showed that with 8 projections the DART reconstruction exhibited similar artifacts. For the multi-label phantom we were able to generate a good quality image with only 6 projections. Similarly, all other techniques exhibited more artifacts with 6 projections.

We then added white Gaussian noise to observations resulting in a SNR of 20 dB. The performance plots are shown in Fig. 2 (b) and (d) for the binary and multi-label phantoms, respectively. We observe that the performance of all the reconstruction techniques degrade and good quality reconstructions require more projections compared to the noise free case. Example reconstructions are shown in Fig. 5 using 12 and 8 projections for the binary and multi-label phantoms respectively.

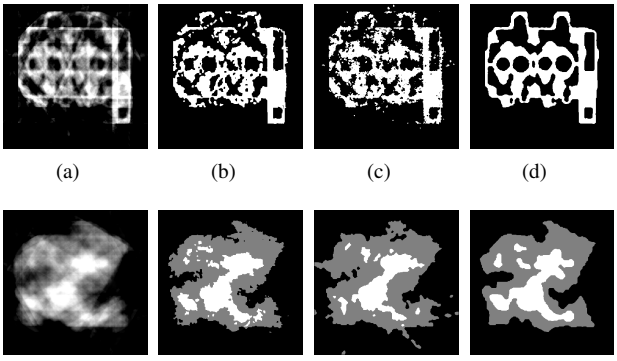

(a) (b) (c) (d)

(e) (f) (g) (h)

Figure 4. *Sparse angle reconstruction without noise: Binary and multi-label phantoms using 8 and 6 projections, respectively. (a), (e) SART. (b), (f) DART. (c), (g) GCWSA. (d), (h) TOMO-SPL. FBP results were left out due to space limitations.*

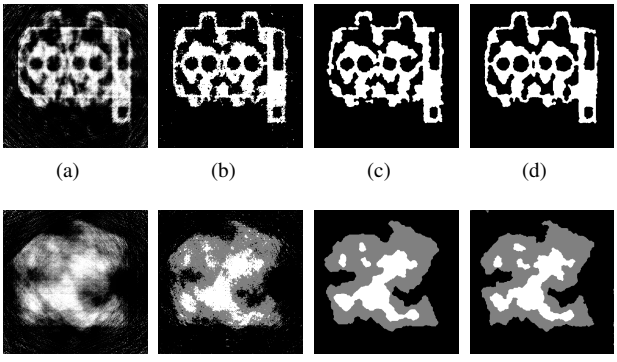

(a) (b) (c) (d)

(e) (f) (g) (h)

Figure 5. *Sparse angle reconstruction with observation noise (20 dB SNR): Binary and multi-label phantoms using 12 and 8 projections, respectively. (a), (e) SART. (b), (f) DART. (c), (g) GCWSA. (d), (h) TOMO-SPL. FBP results were left out due to space limitations.*

Limited Angle Experiments

Limited angle scenarios are usually more challenging since they do not offer distinct projections of the underlying field. As a result very few observations are available for certain regions of the underlying field. In limited angle scenarios, the angular span was sampled at every 1°. Here we only focus on reconstruction from noisy data. White Gaussian noise was added to observations resulting in a SNR of 20 dB.

The performance of the compared techniques over the angular range is illustrated in Fig 3 (b) and (c). TOMO-SPL outperforms GCWSA, DART and the conventional techniques by yielding a more reliable representation of the underlying scene in all measurement scenarios. The advantage of TOMO-SPL is even

more striking when reconstructing the multi-label image from 60° angular span. In this case the error of TOMO-SPL is 3 times smaller than its closest competitor. It was also reported by [10] that although DART has good reconstruction performance under low noise scenarios, its performance degrades under noise. This can be attributed to the fact that DART does not have a principled regularization framework. GCWSA was unable to recover the objects at lower angular spans. The authors have observed this behavior previously for the multi-label phantom noting that they were not able to generate a good reconstruction below 120° in [10]. In comparison, TOMO-SPL was able to generate a faithful representation at 70°. Sample reconstructions with 90° span for the binary phantom and 70° span for the multi-label phantom are shown in Fig.6. TOMO-SPL yielded more accurate representations of the underlying fields with low angular coverage in the presence of measurement noise compared to other techniques.

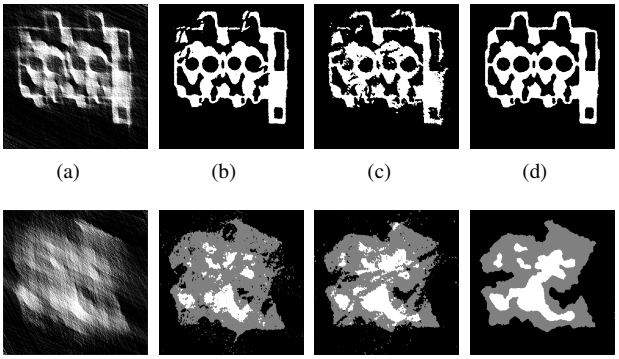

(a) (b) (c) (d)

(e) (f) (g) (h)

Figure 6. *Reconstruction of binary and multi-label phantoms using projection data from 90° and 70° limited angle observations, respectively. White Gaussian noise is added to the observations resulting in 20 dB SNR. (a), (e) SART. (b), (f) DART. (c), (g) GCWSA. (d), (h) TOMO-SPL. FBP results were left out due to space limitations.*

Conclusions

In this work, we further develop and examine the variable splitting approach for the discrete tomography problem proposed in [11]. This framework provides a method to solve regularized discrete valued computational imaging problems. The solution is obtained exploiting the ADMM technique. We tested and compared the performance of the proposed TOMO-SPL technique to a variety of existing conventional and a state of the art reconstruction method in sparse and limited angle tomography examples. We showed that the proposed method yields a reliable representation of the underlying field under challenging data collection scenarios.

References

[1] Downing, K. H., Sui, H., and Auer, M., "Electron tomography: A 3D view of the subcellular world," *Analytical Chemistry* **79**(21), 7949–7957 (2007).

[2] Fishburn, P., Schwander, P., Shepp, L., and Vanderbei, R. J., "The discrete Radon transform and its approximate inversion via linear programming," *Discrete Applied Mathematics* **75**(1), 39 – 61 (1997).

[3] Weber, S., Schnorr, C., and Hornegger, J., "A linear programming relaxation for binary tomography with smoothness priors," *Electronic Notes in Discrete Mathematics* **12**(0), 243 – 254 (2003). 9th International Workshop on Combinatorial Image Analysis.

[4] Batenburg, K. and Sijbers, J., "DART: A practical reconstruction algorithm for discrete tomography," *IEEE Trans. on Image Processing* **20**, 2542 –2553 (sept. 2011).

[5] Bleichrodt, F., Tabak, F., and Batenburg, K., "SDART: An algorithm for discrete tomography from noisy projections," *Computer Vision and Image Understanding* **129**, 63 – 74 (2014). Special section: Advances in Discrete Geometry for Computer Imagery.

[6] Boykov, Y. and Funka-Lea, G., "Graph cuts and efficient N-D image segmentation," *International Journal of Computer Vision* **70**, 109–131 (2006). 10.1007/s11263-006-7934-5.

[7] Raj, A. and Zabih, R., "A graph cut algorithm for generalized image deconvolution," in [*In ICCV*], 1048–1054 (2005).

[8] Rother, C., Kolmogorov, V., Lempitsky, V., and Szummer, M., "Optimizing binary MRFs via extended roof duality," in [*Computer Vision and Pattern Recognition, 2007. CVPR '07. IEEE Conference on*], 1 –8 (june 2007).

[9] Kappes, J., Petra, S., Schnr, C., and Zisler, M., "Tomogc: Binary tomography by constrained graphcuts," in [*Pattern Recognition*], Gall, J., Gehler, P., and Leibe, B., eds., *Lecture Notes in Computer Science* **9358**, 262–273, Springer International Publishing (2015).

[10] Tuysuzoglu, A., Karl, W., Stojanovic, I., Castanon, D., and Unlu, M., "Graph-cut based discrete-valued image reconstruction," *Image Processing, IEEE Transactions on* **24**, 1614–1627 (May 2015).

[11] Tuysuzoglu, A., Khoo, Y., and Karl, W. C., "Variable splitting techniques for discrete tomography," in [*2016 IEEE International Conference on Image Processing (ICIP)*], 1764–1768 (Sept 2016).

[12] Xu, Z., De, S., Figueiredo, M. A. T., Studer, C., and Goldstein, T., "An empricial study of ADMM for nonconvex problems," in [*NIPS 2016 Workshop on Nonconvex Optimization for Machine Learning: Theory and Practice*], (2016).

[13] Kovnatsky, A., Glashoff, K., and Bronstein, M. M., "MADMM: a generic algorithm for non-smooth optimization on manifolds," *arXiv:1505.07676* (2015).

[14] Jia, K., Chan, T.-H., Zeng, Z., Gao, S., Wang, G., Zhang, T., and Ma, Y., "ROML: A robust feature correspondence approach for matching objects in a set of images," *arXiv:1403.7877* (2015).

[15] Hochbaum, D. S., "An efficient algorithm for image segmentation, Markov random fields and related problems," *J. ACM* **48**, 686–701 (jul 2001).

[16] Komodakis, N. and Tziritas, G., "Approximate labeling via graph cuts based on linear programming," *Pattern Analysis and Machine Intelligence, IEEE Transactions on* **29**, 1436–1453 (Aug 2007).

[17] Komodakis, N., Tziritas, G., and Paragios, N., "Performance vs computational efficiency for optimizing single and dynamic mrfs: Setting the state of the art with primal-dual strategies," *Comput. Vis. Image Underst.* **112**, 14–29 (Oct. 2008).

[18] Glowinski, R. and Marroco, A., "Sur l'approximation, par éléments finis d'ordre un, et la résolution, par pénalisation-dualité d'une classe de problèmes de dirichlet non linéaires," *Revue française d'automatique, informatique, recherche opérationnelle. Analyse numérique* **9**(2), 41–76 (1975).

[19] van Aarle, W., Palenstijn, W. J., Beenhouwer, J. D., Altantzis, T., Bals, S., Batenburg, K. J., and Sijbers, J., "The {ASTRA} toolbox: A platform for advanced algorithm development in electron tomography," *Ultramicroscopy* **157**, 35 – 47 (2015).

[20] Batenburg, K. J., van Aarle, W., and Sijbers, J., "A semi-automatic

algorithm for grey level estimation in tomography," *Pattern Recogn. Lett.* **32**, 1395–1405 (July 2011).

[21] Otsu, N., "A Threshold Selection Method from Gray-level Histograms," *IEEE Transactions on Systems, Man and Cybernetics* **9**(1), 62–66 (1979).